The biological properties of the silver- and copper-doped ceramic biomaterial

Oleksandr Lysenko, Oleksii Dubok, Anatolii Borysenko & Oleksandr Shinkaruk

Journal of Nanoparticle Research
An Interdisciplinary Forum for
Nanoscale Science and Technology

ISSN 1388-0764
Volume 17
Number 4

J Nanopart Res (2015) 17:1-15
DOI 10.1007/s11051-015-2971-z

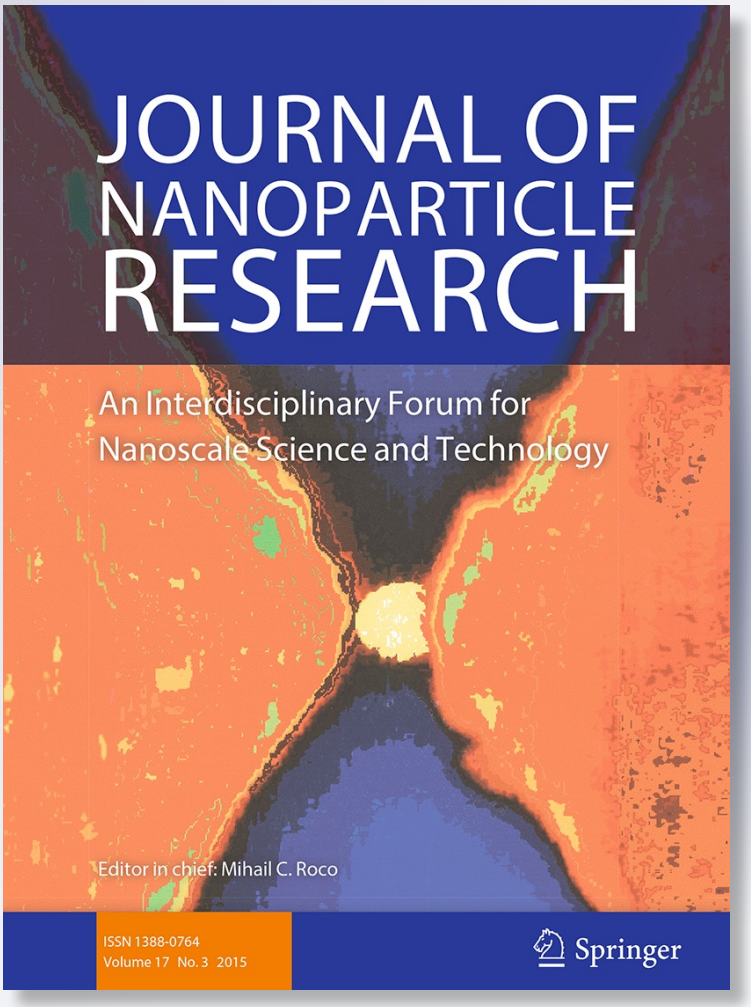

Springer

Journal of Nanoparticle Research
All Volumes & Issues
ISSN: 1388-0764 (Print) 1572-896X (Online)

In this issue (36 articles)

1. Research Paper

   Mechanistic studies for depositing highly dispersed Pt nanoparticles on carbon by use of trimethyl(methylcyclopentadienyl)platinum(IV) reactions with O_2 and H_2

   Alia M. Lubers, *Christopher L. Muhich*... Article:179

2. Research Paper

   Topical Collection

   The biological properties of the silver- and copper-doped ceramic biomaterial

   Oleksandr Lysenko, *Oleksii Dubok*, *Anatolii Borysenko*... Article:178

3. Research Paper

   Workplace performance of a loose-fitting powered air purifying respirator during nanoparticle synthesis

   Antti J. Koivisto, *Mikko Aromaa*, *Ismo K. Koponen*... Article:177

4. Research Paper

   Role of surface in high photoconductive gain

measured in ZnO nanowire-based photodetector

Bhargav Mallampati, *S. V. Nair*, *H. E. Ruda*... Article:176

5. Research Paper

Bioavailability of Zn in ZnO nanoparticle-spiked soil and the implications to maize plants

Xueqin Liu, *Fayuan Wang*, *Zhaoyong Shi*, *Ruijian Tong*... Article:175

6. Research Paper

Nanoscale mixing during double-flame spray synthesis of heterostructured nanoparticles

H. K. Grossmann, *T. Grieb*, *F. Meierhofer*, *M. J. Hodapp*... Article:174

7. Research Paper

Preparation of carbon-coated $MnFe_2O_4$ nanospheres as high-performance anode materials for lithium-ion batteries

Fei Jiang, *Xiumei Du*, *Saihua Zhao*, *Jinxin Guo*... Article:173

8. Research Paper

Toxicity of silver nanoparticles against bacteria, yeast, and algae

Loredana S. Dorobantu, *Clara Fallone*, *Adam J. Noble*... Article:172

9. Research Paper

Experimental determination of the steady-state charging probabilities and particle size conservation in non-radioactive and radioactive bipolar aerosol chargers in the size range of 5–40 nm

Peter Kallinger, *Wladyslaw W. Szymanski* Article:171

10. Research Paper

Segregation phenomena in Nd–Fe–B nanoparticles

F. Schmidt, *D. Pohl*, *L. Schultz*, *B. Rellinghaus* Article:170

11. Research Paper

Field emission current from a junction field-effect transistor

Mahta Monshipouri, *Yaser Abdi* Article:169

12. Research Paper

Therapeutic potential of inhibiting ABCE1 and eRF3 genes via siRNA strategy using chitosan nanoparticles in breast cancer cells

Bagdat Burcu Cengiz, *Mehmet Dogan Asik*, *Goknur Kara*... Article:168

13. Research Paper

Preparation and in vitro characterization of gallic acid-loaded human serum albumin nanoparticles

Hossein Mohammad-Beigi, *Seyed Abbas Shojaosadati*... Article:167

14. Research Paper

Soft chemistry synthesis route toward Bi_2Te_3 hierarchical hollow spheres

J. Fouineau, *J. Peron*, *S. Nowak*, *M. Giraud*, *M. Sicard*... Article:166

15.

Research Paper

Facilitated transport of titanium dioxide nanoparticles by humic substances in saturated porous media under acidic conditions

Ruichang Zhang, *Haibo Zhang*, *Chen Tu*, *Xuefeng Hu*... Article:165

16. 

Research Paper

Effect of solvent and silicon substrate surface on the size of iron nanoparticles

Phillip Newman, *Adriyan Milev*, *Kamali Kannangara*... Article:164

J Nanopart Res (2015) 17:178
DOI 10.1007/s11051-015-2971-z

RESEARCH PAPER

The biological properties of the silver- and copper-doped ceramic biomaterial

Oleksandr Lysenko · Oleksii Dubok · Anatolii Borysenko · Oleksandr Shinkaruk

Received: 31 October 2014 / Accepted: 17 March 2015

Abstract The biological properties of nanostructured bioactive ceramic composite (BCC) granules doped with 0.1–10 at.% silver and 0.05–5 at.% copper have been investigated both in vitro and in vivo to develop effective alloplastic material for infected bone defect substitute. It is assumed that the granules consisting of biphasic calcium phosphate and bioactive glass ceramics due to their nanoscale (15–40 nm) and multiphase structure, bioelement placement in different ceramic phases as well as antimicrobial effect should improve osteogenic properties and biocompatibility. Tests in vitro have been conducted with multipotent mesenchymal stromal cells (MSCs) and test strains of microorganisms. The same biocomposite has been used in vivo to study the repair of bone defects in animal model. The findings indicate that doped BCC leads to antimicrobial activity. Inhibition of MSCs growth has been observed for granules doped with ions of more than 1 at.% silver and 0.5 at.% copper. The results of the in vivo study reveal that BCC implantation significantly improves bone reparation. Differences between bone repair with undoped and doped, with 1 at.% silver and 0.5 at.% copper, ceramic samples were not observed. The BCC doped within 0.5–1 at.% silver and 0.25–0.5 at.% copper stimulates bone tissue repair and has satisfactory biocompatibility and antimicrobial properties.

Keywords Bioactive ceramics · Nanocrystallinity · Silver and copper · Antimicrobial · Cytotoxicity · Osteogenesis · Bioinspired nanomaterials

Guest Editor: Liudmyla Rieznichenko

This article is part of the topical collection on Engineered Bioinspired Nanomaterials

O. Lysenko (✉) · A. Borysenko
Department of Therapeutic Stomatology, Bogomolets National Medical University, 34 Peremohy Av., Kyiv 01601, Ukraine
e-mail: dr.alex.lysenko@gmail.com

O. Dubok · O. Shinkaruk
Department of Analytical Chemistry and Functional Ceramics, Institute for Problems of Material Science NASU, 3 Krzhizhanovsky Str., Kyiv 03142, Ukraine

O. Dubok
Department of Inorganic Chemistry, Faculty of Chemistry, National Taras Shevchenko University of Kyiv, 64 Volodymyrska Str., Kyiv 01601, Ukraine

Introduction

Today, bioactive ceramics consists of a large group of materials including calcium phosphate ceramics, bioactive glasses, and glass ceramics. All bioactive ceramics have proved to be the key elements of contemporary bone reconstruction surgery, revealing high effectiveness in bone tissue restoration. The promising and important task at present is functionalization of these materials that means a modification of their composition, structure, and properties to solve specific problems in various fields of bone surgery. In

Published online: 10 April 2015

particular, in maxillofacial, dental practice and for many cases of bone injuries, it is difficult to avoid infection of the surgical field (Heitz-Mayfield et al. 2006; Dodwad et al. 2012). Therefore, the bone grafts used for such surgeries should besides of the usual set of requirements for bone substitutes materials provide anti-inflammatory and antibacterial action for many kinds of pathogenic microflora and at the same time the absence of inhibition of reparative processes in the bone tissue.

Currently, multi-doped bioactive ceramics are increasingly becoming an area of great interest (Shepherd et al. 2012). Contemporary state of knowledge allows to significantly modify conventional calcium phosphate ceramics in order to diversify their biological properties and use them as the bases for multifunctional systems. Porosity regulation (Hsu et al. 2007; Munch et al. 2008), nanosize structuring (Dorozhkin 2010), insertion of additional ceramic phases, and hydroxyapatite (HAp) ion substitution (Porter et al. 2004; Sogo et al. 2004; Chen et al. 2007; Landi et al. 2008; O'Donnell et al. 2008; Spence et al. 2009) are among the possible options.

For instance, conjunction of macro- and microporosity of a bioactive ceramics improves graft osteoconductivity, and such ceramics may serve as a carrier for stromal and stem cells (Sanchez-Salcedo et al. 2006; Eniwumide et al. 2007; Balagna et al. 2011). Nanostructuring of HAp increases its surface area, improves osteointegration and rate of biodegradation (Dorozhkin 2010), and due to hydrophilicity of the material enables to use the graft for absorption and directional delivery of a variety of medical preparations in large amounts. (Fan et al. 2007; Thanyaphoo and Kaewsrichan 2012).

Incorporation into the structure of bioactive ceramics such elements as zinc, copper, or silver imparts it antibacterial properties (Shepherd et al. 2012; Jaiswal et al. 2012). Since ancient times, silver and copper have been used as antibacterial agents, especially before advent of antibiotics in 20th century. However, the entire mechanism of their influence on prokaryote and eukaryote cells is still unclear. Development of bacteria resistance to the action of heavy metals has been reported (Balamurugan et al. 2008; Marambio-Jones and Hoek 2010). Since frequent commercial uses of silver and copper particles to fight infection, widespread silver resistance is a growing concern. Silver (and other heavy metals) resistance in bacteria is often encoded by plasmids genes, as for example the *Salmonella* plasmid pMG101, within the IncHI incompatibility group, as well as in other five plasmids in the same group (Gupta et al. 2001). Doping of bioactive ceramics with copper besides its antibacterial properties may stimulate osteo- and angiogenesis (Barralet et al. 2009; Lüthen et al. 2010; Ewald et al. 2012; Wu et al. 2013).

However, there are no references as for biological properties of bioactive ceramics with combined silver, copper, or zinc ion doping although toxic effects of these elements on human body and cells have been reported (Marambio-Jones and Hoek 2010). Most of the toxicity data presented in the literature are obtained in relatively simple media like water or cell culture media, which do not reflect the aquatic environment inside living organisms. Hence, these data may not be relevant for assessing behavior in real systems.

The present study aims to optimize bone reparative properties and antimicrobial activity of bioactive ceramic bone substitute to contribute to effective bone surgery grafting material development. The relevant specific functionalization of the ceramics has been achieved through optimizing structure, chemical and phase composition of the ceramics, and selective doping of components with silver, copper, and zinc to maintain balance between the bone remodeling effect and toxicity. Comprehensive pre-biological (XRD, XPS, TEM, ICP) investigations, in vitro, and in vivo studies have been carried out for the ceramics with different dopant concentrations to reconcile antimicrobial properties and cytotoxic with the best action on bone defect healing in animal model.

Materials and methods

Bioactive ceramic composite preparation

The bioactive ceramic composite (BCC) used in this study consisted of a mixture of bioactive glass ceramic (BG) granules with composition of $37SiO_2$–$36CaO$–$13P_2O_5$–$3MgO$–$0.5K_2O$–$4.5ZnO$–$6B_2O_3$ (wt%) and biphasic calcium phosphate (BCP) ceramic granules doped with different amounts of silver and copper. To produce BCC for bone defect filling, these granules were uniformly mixed together at the weight ratio of 70:30.

Compositions of the studied samples are presented in Table 1.

Table 1 The bioactive ceramic composite samples obtained during synthesis

Sample symbol	Sample composition	Nominal dopants concentration (at.%)	
		Silver (Ag^{+})	Copper (Cu^{2+})
BCC1	BCP (30 %), BG (70 %)	0.1	0.05
BCC2		0.5	0.25
BCC3		1	0.5
BCC4		2	1
BCC5		10	5
BCC		Control, undoped sample	

To produce the samples, the following methods have been used:

Synthesis of the bioactive glass ceramics

Bioactive glass ceramics was synthesized by melting in air. The starting reagents (salts or oxides) in the calculated quantities were thoroughly mixed in a porcelain drum with grinding balls, then compacted by pressing, calcined to remove volatiles at 800 °C, and melted at 1300 °C. The melted ingot of the glass ceramics was crushed, ground, and sieved through a sieve with a mesh size of 800 and 300 microns to produce the selected particle sizes (315–800 μm).

Synthesis of BCP ceramics

BCP ceramics was synthesized via decomposition of calcium-deficient non-stoichiometric hydroxyapatite (CDHA). The latter was prepared by chemical precipitation at reaction

$$(10-x)\ \mathrm{Ca(NO_3)_2}+6(\mathrm{NH_4})_2\mathrm{HPO_4} = \mathrm{Ca_{10-x}(PO_4)_6(OH)_2} + (20-2x)\mathrm{NH_4NO_3} + 6\mathrm{H_2O}.$$

The precipitate of the reaction was washed, dried at 100 °C, compacted by pressing, sintered at 1000 °C for 1.5 h, and grounded to produce granules with desired size, which were further used for silver and copper co-doping.

Doping with silver and copper

Antimicrobial properties of the ceramic composite were attained by doping the BCP ceramic granules with silver and copper at the atomic ratio of Ag/Cu = 2:1. The ranges of silver and copper concentrations selected for the study were accordingly 0.05–5 and 0.1–10 at.% of the amount of calcium ions in the BCP granules, respectively. The method of doping consisted in heating BCP granules in silver and copper nitrates solution with calculated concentrations under stirring until complete solution evaporation followed by drying at 120 °C and heat treatment at 700 °C for 6 h. The complete decomposition of silver and copper nitrates and the removal of nitrogen oxides and solid-state diffusion of the impurities from the surface into the granules to form solid solution took place during the heat treatment. Comparing ionic radii and electronegativity, we could expect a substitutional model of solid solution with replacement of calcium places by silver and copper.

For sterilization, the BCC samples were autoclaved for 1 h at 180 °C prior to biological tests.

Study of the physical and chemical properties

XRD The phase compositions of the samples were studied by X-ray diffraction with DRON-3M diffractometer, using Cu Kα radiation at the wavelength of 1.5418 Å. The patterns were registered in the 2θ range of 15–60° with a step size of 0.1° and measuring time of 4 s per step.

XPS X-ray photoelectron spectra were measured with photoelectron spectrometer JSPM-4610 (JEOL) using a non-monochromatic Mg Kα (1253.6 eV) X-ray source. The vacuum in the analysis chamber was 10^{-7} Pa and the accuracy of the electron binding energy measurement was 0.1 eV. To neutralize the charge accumulating at insulating sample during the experiment, its surface has been coated with a thin layer of carbon. To calibrate the X-ray photoelectron spectra, the binding energy of the C 1 s (284.0 eV) or O 1 s (530.4 eV) has been used.

TEM was performed using a JEOL JEM-2100F operated at 200 kV.

AES-ICP The doping process of biphasic granules was checked with ICP instrument (AES-ICP, Spectroblame Modula ICP "Spectro"). The composition of the second component of the composite, bioactive glass ceramics was fully controlled by the initial charge.

Study of the biological properties

Assessment of test microorganism susceptibility

The referent strains of gram-positive and gram-negative bacteria and *Candida* fungi with different taxonomic positions such as *Staphylococcus aureus* (ATCC 25923), *Escherichia coli* (ATCC 25922), *Pseudomonas aeruginosa* (ATCC 27853), and *Candida albicans* (ATCC 885-653) were used as test organisms. All microorganisms in the study had been received from the Museum of Vital Cultures Laboratory of General Microbiology, the Institute of Epidemiology and Infectious Disease, Kyiv, Ukraine and grown in the individual prescribed medium. The antimicrobial properties were evaluated by standard method of cell culture dishes. Standard Petri dishes (10 cm diameter) placed on strictly horizontal surface were filled with two layers of solid nutrient media, the lower layer (10 mm) being pure melted Mueller-Hinton Agar (HiMedia, India), and the upper layer being meant for the respective day's test microorganism culture, namely Peptone Nutrient Agar (LabSnab, Ukraine) for *E. coli* and *P. aeruginosa,* Peptone Nutrient Agar with 1 % glucose (LabSnab, Ukraine) for *S. aureus,* and Saburo Agar (VWR Prolab, USA) for *C. albicans.* After the agar lower layer was cooled, thin-walled hollow cylinders with inner diameter of 6 mm were installed at equal distances to one another and to the Petri dish edge. The nutrient medium mixed with the test microorganism inoculation dose (1.5 ml of microbe dredge) was melted and cooled to 45–48 °C, and was poured around the cylinders. After cooling the agar upper layer, the cylinders were removed and the remaining holes were filled with equal amounts (55 mg) of the BCC sample granules under study. Results were estimated after 24 h keeping at 37 °C in thermostat. Antimicrobial activity assessment was made by the size of the microorganism growth inhibition area around each ceramic sample (in mm) including holes. At the same time, medium sterility and microorganism growth in ceramics-free environments were monitored. The obtained results were evaluated by the following criteria:

- 6 mm diameter of growth inhibition area was assessed as no antimicrobial effect;
- 7–14 mm area diameter—as a slight antimicrobial effect;
- 15–19 mm area diameter—a moderately expressed antimicrobial effect; and
- 20 mm or more area diameter—as a high antimicrobial effect.

Assessment of cytotoxicity in human cell culture

Biocompatibility and cytotoxic effects of the ceramic composite were studied in the native culture of human adipose-derived multipotent mesenchymal stromal cells (AD-MSCs) at third passage (P3). The human cell culture was obtained from the Cell and Tissue Technologies Unit, State Institute of Genetic and Regenerative Medicine of NAMS (Kyiv, Ukraine). Multipotent mesenchymal stromal cells (MSCs) are understood as plastic adherent cell faction from any connective tissue stroma meeting certain criteria (Dominici et al. 2006). The direct (DCT) and indirect (ICT) cytotoxicity tests were done according to recommendations of the ISO 10993 standard (International Organization for Standardization (ISO) 2009).

For ICT every BCC, sample has been previously sterilized by dry heat for 60 min at 180 °C and in an amount of 0.1 g BCC per well ($S = 9.6$ cm^2), placed into the wells of 6-well cell culture plate (Costar, USA) and filled each well with a BCC sample with growth medium: DMEM:F12 (Sigma-Aldrich, USA) supplemented with 10 % fetal calf serum (Sigma-Aldrich, USA), 100 IU/ml penicillin and streptomycin (Darnitsya, Ukraine), 2 mM L-glutamine (Sigma-Aldrich, USA), and left in a multi-gas incubator (Binder, Germany) over 24 h at 37 °C and 5 % CO_2 atmosphere for BCC diurnal extract production for ICT. Further, the BCC extracts have been aspirated from each well and in the amount of 20 % these extracts were added to fresh growth medium. Human-cultured AD-MSCs at P3 were seeded in a number of 3.0×10^4 ($\sim 3.1 \times 10^3$ cells/cm^2) per well per BCC extract as follows: by six wells with 3.0×10^4 cells

per each BCC extract and six control wells with only cell culture.

To determine direct cytotoxicity, we studied the effect of the BCC granules (0.1 g) which were in direct contact with cell culture monolayer. Dry heat-sterilized BCC granules were placed into the 6-well cell culture plate (Costar, USA) with growth medium and AD-MSC culture monolayer ($\sim 3.1 \times 10^3$ cells/cm^2) according to the previous scheme. Then the inoculated plates were left in a multi-gas incubator (Binder, Germany) for 3 days at 37 °C and 5 % CO_2 atmosphere. The possible influence of BCC sample components (with alkalinity or acidity beyond physiological) on pH-dependent growth medium color change was also studied. The growth medium contained a Phenol Red coloring agent, red at physiological pH values of 7.2–7.4, going violet with rising alkalinity or yellow with rising acidity.

To identify cells over the optically dense BCC sample granules, the method of intravital cell suspension staining with fluorescein diacetate solution, FDA (Sigma-Aldrich, USA), was applied to growth medium within 5 min at room temperature using the amount of 1 ml of working solution (5 μmol/L) of the coloring agent per well. After that the solution was poured off, and the culture was washed and left in Dulbecco's phosphate-buffered saline, DPBS (PAA, Austria) to be immediately microscoped. Viable cells were identified by their fibroblast-like morphology and green fluorescence at $I_{ex} = 450$–490 nm, $I_{em} = 520$ nm with filter set 09 (Carl Zeiss, Germany).

Visualization by means of inverted microscopy in transmitted light, phase contrast microscopy, and fluorescent microscopy and *cell culture photo-registration* were conducted with inverted fluorescent Axio Observer A1 microscope, ZEN lite 2011 (blue edition) picture processing software, Axio Cam ERc 5s digital camera (Carl Zeiss, Germany). Cell cultures were microscoped within one hundredfold increase. Thus, on the third day, it was possible to calculate the total number of viable and dead cells in each hole of the respective group using a standard hemocytometer.

Study of the effect on experimental bone defect reparation

As experimental animals for the in vivo study, the population of 56 white female Wistar rats at the age of 12 months and with average live weight of 330 ± 15 g was taken. The rats were divided into four groups. The first group included eight intact rats assumed to be physiologically normal. The second group included 16 animals with experimentally created unsubstituted mandible defect, the third group consisted of 16 rats with the BCC suspension bone defect filled, and the fourth group included 16 animals with bone defects filled with the suspension of ceramic composite doped with 1 at.% silver and 0.5 at.% copper (BCC3). The bone tissue defects were created under thiopental anesthesia (20 mg/kg) following the surgical site denudation and antiseptic application. The 1.5–2 cm incision was made through the skin, subcutaneous tissue and fascia at 0.5 cm from the mandible edge followed by blunt penetration to the mandible body and angular process, where periosteum was elevated. Round through defect was created with 4-mm inverted-conical dental drill in the mandibular bone thickest place approximately at the margin of alveolar part and the bone body followed by cooling liquid (saline) irrigation. Undoped BCC suspension was pluggered into the bone defect in the rats of the 3rd group, while in the 4th group, animals received BCC3. The periosteal flap was replaced, and the wound was sutured layer by layer. The suspensions were prepared *ex tempore* in sterile surgery crucible by adding salt solution after pounding the granules.

The experimental animals were kept and involved in the experiment procedures according to the "Law on Protection of Animals from Cruel Treatment" No 1759-VI of 15, December 2009 currently in force in Ukraine and with regard to the European Convention for the Protection of Vertebrate Animals Used for Experimental and Other Scientific Purposes (Strasbourg European Convention).

Eight rats from groups 2–5 were euthanized on the 10th day of the experiment under thiopental anesthesia (20 mg/kg), whereas the other eight rats from each group were euthanized on the 30th day. Phlebotomy was used in each case.

Alkaline phosphatase (AlP), acid phosphatase (AP), and elastase activity as well as AlP/AP ratio (mineralization index), general proteolytic activity (GPA) by casein hydrolysis at pH 7.6, and soluble protein content by Lowry method (Stoscheck 1990) were determined in bone tissue homogenates (75 mg/ml 0.1 M of pH 6.1 citrate buffer). Calcium and phosphorus contents were assessed in bone tissue

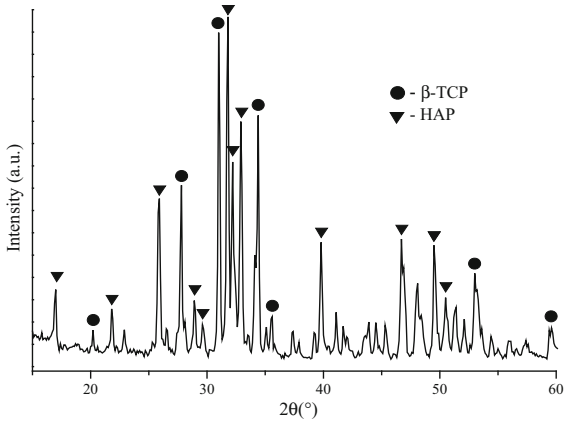

Fig. 1 The XRD pattern of the pure undoped sample of the BCP ceramics, calcined at 1000 °C

homogenates prepared on 0,1 N of HCl solution on the basis of 50 mg/ml. Calcium content/soluble protein concentration ratio (Ca/prot.) was estimated by the following formula:

$$\text{Ca/prot.} = \frac{C_{\text{Ca}} \times 40}{C_{\text{prot.}}},$$

where C_{Ca} is the calcium content in mol/kg and $C_{\text{prot.}}$ is the protein content in g/kg.

The collagen-forming index was calculated by GPA/elastase ratio, reflecting the activity of a number of proteases, some of them being relative to collagen formation from its predecessor and leucocytic elastase affecting collagen degradation rate. In order to study histological regenerate structure, the excised alveolar process bone tissue in the defect area with surrounding tissue of animals from all groups was fixed in the neutral formaldehyde solution. Following decalcification in hydrochloric acid by Ebner method, it was gradually dehydrated in alcohols of a different dehydration capacity and fixed in paraffin (Bancroft and Stevens 1990). The deparaffinized and dehydrated 10–12-μm-thick slices were stained with hematoxylin and eosin. Histological examination was made with Jenamed 2 microscope (Jenoptik AG, Germany). Images were registered with Canon EOS 5D digital camera (Canon Inc., Japan). The study protocol was reviewed and approved by the Ethics Committee in Kyiv, Bogomolets National Medical University, Ukraine (reference number 82/081014).

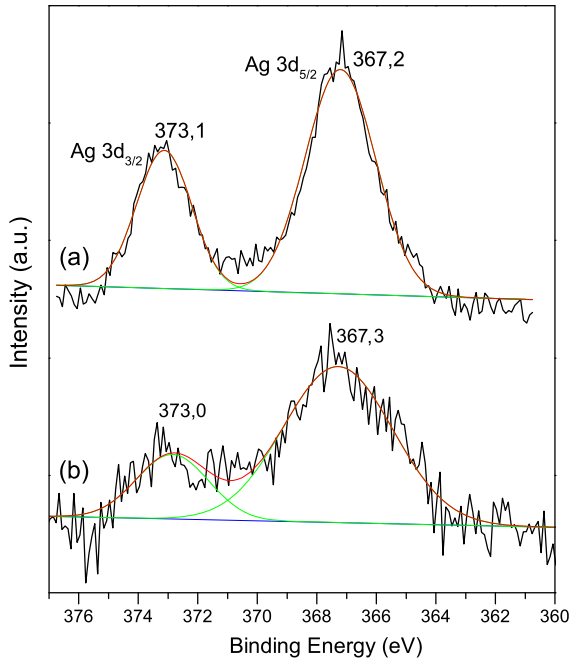

Fig. 2 Ag 3d XPS spectra of BCC5 (**a**) and BCC3 (**b**)

Statistical analysis

For data processing and statistical evaluation, appropriate validated software was used Statistica software package, version 10.1, StatSoft Inc., Tulsa, OK, USA. Descriptive summary statistics were computed for all parameters documented. Group mean (M) ± m (SE, standard error) was calculated for each test parameter. Between-group differences at the beginning and the corresponding period of the experiments were tested using the unpaired *t-test*. The significance level was set at $P < 0.05$ for all group comparisons.

Results and discussion

Sample characterization

XRD The washed and dried precipitate of CDHA had a defective crystalline structure of HAp with broadened reflections, but after compacting by pressing and sintering at 1000 °C, the non-stoichiometric HAp was transformed into the composition of two phases—a stoichiometric hydroxyapatite and β-tricalcium phosphate (β-TCP) in almost equal quantities (Fig. 1). The phase transformation occurs uniformly throughout the

entire volume providing nanosized grains of both phases (Daculsi et al. 2003; Chen et al. 2011). The ceramics fragments were crushed and sieved to obtain fractal granules with selected size (300–800 μm).

For all the composite samples, including those with 10 % Ag and 5 % Cu, XRD analysis has not detected any appearance of new phases.

XPS The oxidation states of silver and copper near the surface of the BCC3 and BCC5 samples were studied using X-ray photoelectron spectroscopy. The

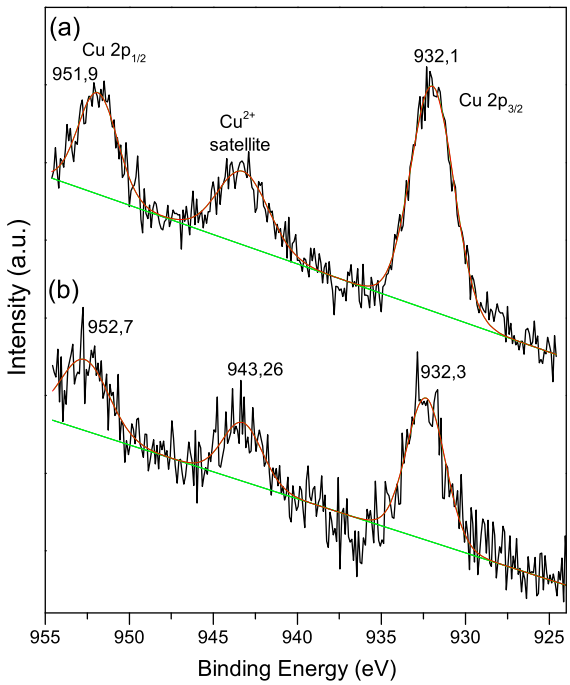

Fig. 3 Cu 2p XPS spectra of BCC5 (**a**) and BCC3 (**b**)

Ag $3d_{5/2}$ peak is very sensitive to the valence state of silver. Unlike most metals, the silver 3d electron binding energy decreases in the order of Ag^0–Ag^+–Ag^{2+} (Schön et al. 1973). The best resolution of different Ag valence states occurs at $3d_{5/2}$ peak near 367 eV. In the current study, binding energy of this peak in both samples BCC3 (Fig. 2b) and BCC5 (Fig. 2a) is 367.3 ± 0.1 eV, that is according to the literature (Hammond et al. 1975) corresponds to the Ag^+ state.

The valence state of copper can be identified by 2p electrons. The peaks close to the 952 and 932 eV correspond to the $Cu2p_{1/2}$ and $2p_{3/2}$, respectively (Fig. 3). The broad peak at 943 eV is a characteristic satellite of Cu^{2+} ions, as it is absent for other oxidation states (Parmigiani et al. 1992). Based on the Cu $2p_{3/2}$ peak shape and the ratio of the intensities of this peak and 943 eV satellite, it can be concluded that copper in both samples is present mainly in the form of Cu^{2+} ions.

TEM Figure 4 shows the Transmission Electron Microscopy images of the BCP before (a) and after (b) calcining at a temperature of 1000 °C (1.5 h). As can be seen, particles have inhomogeneous morphology before and after calcination that is common for multiphase powders. Prior to calcination, all the particles are nanosized (15–30 × 40–150 nm). Calcination is accompanied by a significant recrystallization and crystal size growth, which is sufficiently inhomogeneous, as even in this case, the appreciable amount of the particles has a size less than 100 nm.

AES-ICP The composition of the BCP in the BCC3 sample (in wt%) is presented in Table 2.

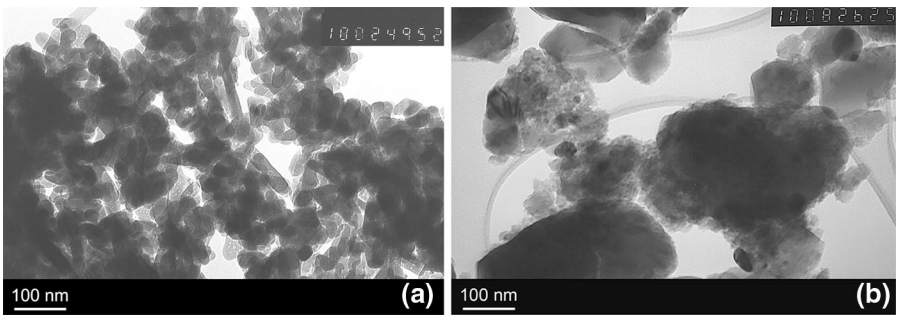

Fig. 4 TEM images of the BCP used in this study: dried at 100 °C (**a**) and calcined at 1000 °C (**b**)

Antimicrobial activity

Doping of the BCC with silver and copper stipulates its antibacterial and antifungal effect (Rameshbabu et al. 2007; Shanmugam and Gopal 2014), and our findings reveals that these effects depend on the microorganism type, dopant concentration and type, structure, and size of the composite granules. The antimicrobial properties of the BCC samples have been found to become more intense with increasing concentrations of dopants. The *E. coli* test strain shows high susceptibility to the dopants in the BCC samples even to the lowest concentration of silver and copper ions (0.1 and 0.05 at.% accordingly). The most resistant test strain turned out to be that of *S. aureus.* Although for the highest concentrations of silver and copper the BCC sample antimicrobial effect was sometimes moderately expressed.

The ceramic composite sample doped with 10 at.% Ag and 5 at.% Cu (BCC5) maximally inhibited the growth of test strains; however, the inhibition was statistically significant ($P < 0.05$) only for *P. aeruginosa* and *C. albican,* whereas the undoped bioactive ceramics never demonstrate any of the effects (Table 3).

The diameter of the inhibition area was more than 27 % at maximum dopant saturation of the ceramic composite (BCC5) compared to the BCC2 sample. As compared to the lower concentrations of silver and copper ions in BCC3 and BCC4 samples, stunting growth of microorganisms was only 17 and 9 % more. Moreover, all growth inhibition areas were clear and distinct (Fig. 5).

Cytotoxic properties

The study shows that in control group (with no ceramic granules present), the number of cultivated cells increased almost by 1.5 times at the third culturing day (Fig. 6).

The ceramic composite containing no silver or copper ions (BCC) did not display any cytotoxic properties and causes no visible inhibition of AD-MSCs. Diffusion of its components into the growth medium neither affected the pH, nor provided for any other inadequate incubation conditions. None of the BCC samples changed the physiological pH value of the growth medium throughout the incubation period, but all BCC samples doped with silver and copper proved to have different cytotoxic properties depending on the dopants concentration. The cytotoxic properties were assessed by direct and indirect methods.

The indirect cytotoxicity test results suggest that the samples under study had no negative effect on cell viability and proliferation. The extracts of the BCC samples doped with 2 at.% silver and 1 at.% copper (BCC4) did not cause cell death on the third culturing day. However, with BCC4 and BCC5 (the highest

Table 2 The result of ICP analysis for the BCP in the BCC3 sample

Element	Ag	Cu	Ca	P	Na	K	Fe	Mg
Concentration (wt%)	0.946 (0.89 at.%)	0.319 (0.5 at.%)	35.615	23.938	0.082	0.008	0.021	0.006

Table 3 Test strain growth inhibition depending on BCC sample (M ± m, mm)

BCC sample	Test strain of microorganism			
	Pseudomonas aeruginosa	*Escherichia coli*	*Staphylococcus aureus*	*Candida albicans*
BCC1	6.0 ± 0.0	10.20 ± 0.32	6.0 ± 0.0	6.0 ± 0.0
BCC2	14.15 ± 0.34	16.70 ± 0.26	13.30 ± 0.46	16.40 ± 0.35
BCC3	17.60 ± 0.16	17.90 ± 0.18	15.15 ± 0.27	18.10 ± 0.72
BCC4	19.80 ± 0.26	18.90 ± 0.82	17.20 ± 0.64	18.4 ± 0.6
BCC5	22.6 ± 0.4	19.20 ± 0.72	17.60 ± 0.95	23.75 ± 0.28
BCC	6.0 ± 0.0	6.0 ± 0.0	6.0 ± 0.0	6.0 ± 0.0

$n = 9$ in each case

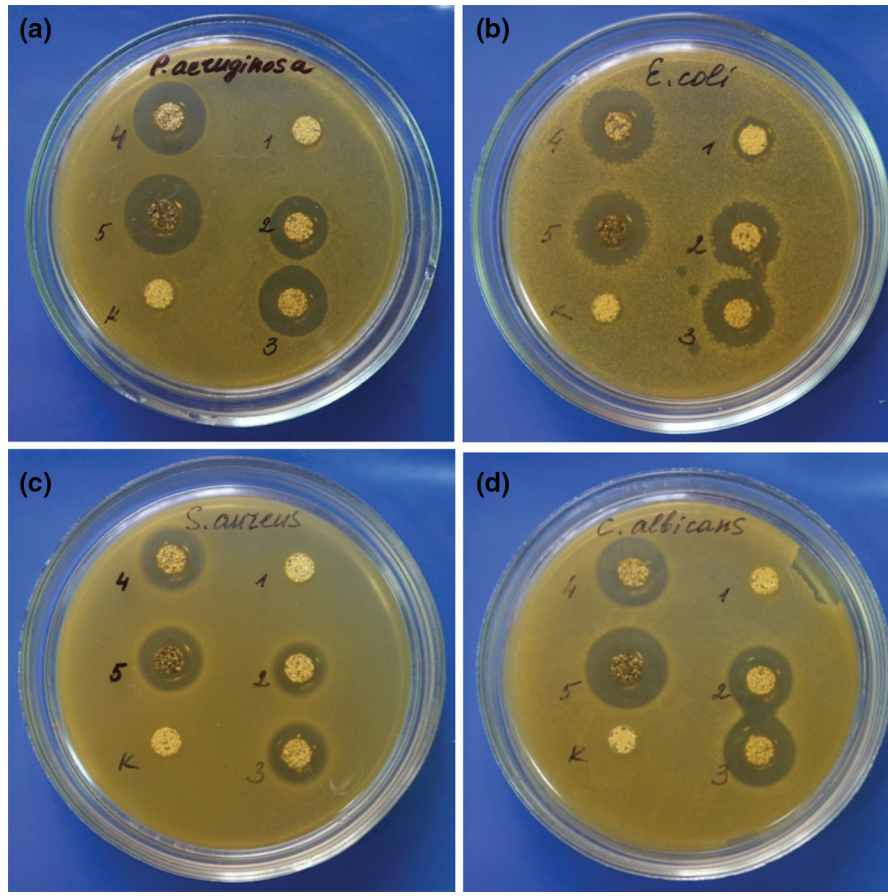

Fig. 5 *P. aeruginosa* (**a**), *E. coli* (**b**), *S. aureus* (**c**), *C. albicans* (**d**) susceptibility to BCC samples 1, 2, 3, 4, 5 with respective silver and copper concentration, K—without additional doping

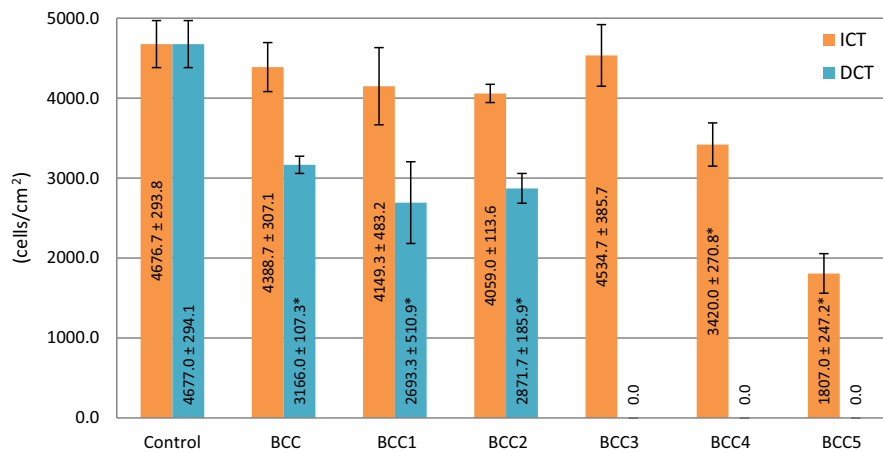

Fig. 6 Assessment of human AD-MSC proliferation according to indirect and direct cytotoxicity tests (M ± m, vital cells), *Notes* $n = 6$ in each BCC group, *— $P < 0.05$ compared to the control

silver and copper concentrations) extracts, the number of cells tended to decrease making it substantially different ($P < 0.05$) from the other samples, while AD-MSCs proliferation in BCC3 was found to be maximum and virtually the same as in control ($P > 0.05$).

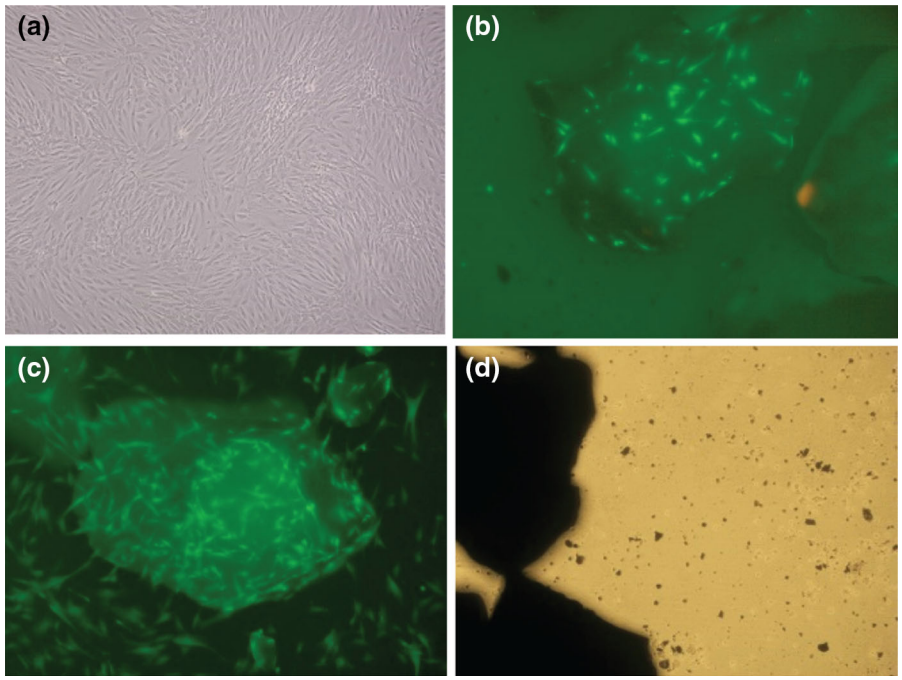

Fig. 7 Microphotography human AD-MSC at P3 cultures—cytotoxicity evaluation of the BCC samples by the direct test (the 3rd day of incubation; ×100; fluorescence microscopy—vital fluorescein diacetate staining): AD-MSCs, monolayer, native preparation—phase contrast microscopy (**a**); AD-MSCs with undoped BCC granules (**b**); AD-MSCs with BCC2 granules (**c**); AD-MSCs with BCC4 granules (dead cells surrounded), native preparation (**d**)

During *the direct test,* the doped BCC samples due to direct contact with the cells reveal increased cytotoxic effect thereby narrowing the cytocompatible range of silver and copper concentrations. For 0.5 at.% silver and 0.25 at.% copper concentrations, ceramic granules (BCC2) neither impeded the culture cells vital activity nor facilitated their proliferation (group 5). Although cell proliferation was decreased in the presence of BCC granules of this group as compared to control, for BCC1 and BCC2 samples, there was no substantial difference ($P > 0.05$) in the number of cells in the holes with the samples on the third culturing day comparing with undoped BCC sample. Destruction of the cell monolayer caused by movement of the BCC granules in the culture-filled holes during transportation of the plates, which hardly has anything to do with the sample cytotoxicity, particularly, in group with BCC, should also be taken into account. Nevertheless, in BCC3, BCC4, and BCC5 groups at the same observation time, the complete cell loss was observed thus demonstrating pronounced ceramic sample direct cytotoxicity (Fig. 7).

The findings can be compared with those reported in literature (Xing et al. 2010; Balagna et al. 2011). The absence of cytotoxic effect of silver and copper ions contained in ceramics on human cells along with their antibacterial activity retained has been established for the cases of insignificant dopant concentrations. Moreover, it has been found that ceramics containing the combination of silver and copper ions has more tangible cytotoxic effect than ceramics with only silver or only copper ions in equal concentration. Combination of silver and copper ions intensifies their antimicrobial properties (Shanmugam and Gopal 2014) and creates pre-conditions for osteo- and angiogenic activity (Wu et al. 2013).

We believe that the optimal concentration of silver and copper ions in bioactive ceramics composites is within 0.5 at.% silver and 0.25 at.% copper. Such dopants concentration (BCC2) does not interfere with adhesion and proliferation of human AD-MSCs, and it may be considered as a cell carrier (Rodriguez et al. 2002) for implantation into the bone tissue.

Table 4 Enzymatic activity, mineral, and dissolved protein content in bone homogenates (M ± m)

No.	Group	Term (days)	AlP (μkat/kg)	AP (μkat/kg)	GPA (nkat/kg)	Elastase (μkat/kg)	GPA/ Elastase	Dissolved Protein (g/kg)	Calcium (mol/kg)	Phosphorus (mol/kg)
1	Intact		25.4 ± 2.6	1.97 ± 0.24	26.8 ± 2.8	5.1 ± 0.5	5.25 ± 0.51	16.8 ± 0.9	2.39 ± 0.12	1.30 ± 0.05
2a	Bone defect, without substitution	10	42.4 ± 3.2	2.36 ± 0.10	46.6 ± 4.7	6.6 ± 0.9	7.06 ± 0.84	19.3 ± 1.3	2.01 ± 0.10	1.21 ± 0.11
			$P < 0.001$	$P > 0.05$	$P < 0.001$	$P > 0.05$	$P < 0{,}05$	$P > 0.05$	$P < 0.05$	$P > 0.3$
3a	Bone defect, BCC	10	74.3 ± 4.7	3.25 ± 0.42	36.9 ± 2.9	6.8 ± 0.3	5.40 ± 0.53	16.1 ± 0.7	2.08 ± 0.15	1.30 ± 0.11
			$P < 0.001$	$P < 0.05$	$P < 0.05$	$P < 0.05$	$P > 0.5$	$P > 0.3$	$P > 0.05$	$P = 1.0$
			$P' < 0.001$	$P' < 0.05$	$P' > 0.05$	$P' > 0.7$	$P' > 0.05$	$P' < 0.05$	$P' > 0.3$	$P' > 0.5$
4a	Bone defect, BCC3	10	73.3 ± 8.2	2.98 ± 0.49	35.3 ± 3.1	6.8 ± 0.6	5.19 ± 0.48	16.5 ± 1.6	2.14 ± 0.05	1.24 ± 0.07
			$P < 0.001$	$P < 0.05$	$P > 0.05$	$P < 0.05$	$P > 0.6$	$P > 0.5$	$P < 0.05$	$P > 0.3$
			$P' < 0.001$	$P' > 0.05$	$P' < 0.05$	$P' > 0.7$	$P' < 0.05$	$P' > 0.05$	$P' > 0.1$	$P' > 0.5$
2b	Bone defect, without substitution	30	21.6 ± 2.5	1.27 ± 0.13	36.1 ± 3.1	5.1 ± 0.5	7.08 ± 0.64	17.9 ± 1.2	2.24 ± 0.02	1.27 ± 0.06
			$P > 0.05$	$P < 0.05$	$P < 0.05$	$P = 1{,}0$	$P < 0.05$	$P > 0.3$	$P > 0.05$	$P > 0.5$
3b	Bone defect, BCC	30	75.1 ± 9.8	2.54 ± 0.49	30.7 ± 2.7	5.9 ± 0.4	5.20 ± 0.53	15.1 ± 1.5	2.12 ± 0.07	1.36 ± 0.07
			$P < 0.001$	$P > 0.3$	$P > 0.3$	$P > 0.2$	$P > 0.7$	$P > 0.3$	$P < 0.05$	$P > 0.3$
			$P' < 0.001$	$P' < 0.05$	$P' > 0.3$	$P' > 0.2$	$P' < 0.05$	$P' > 0.05$	$P' > 0.05$	$P' > 0.3$
4b	Bone defect, BCC3	30	60.3 ± 7.2	1.91 ± 0.10	29.9 ± 2.1	5.5 ± 0.5	5.44 ± 0.57	14.6 ± 1.9	2.27 ± 0.07	1.26 ± 0.08
			$P < 0.001$	$P > 0.3$	$P > 0.3$	$P > 0.4$	$P > 0.5$	$P > 0.2$	$P > 0.3$	$P > 0.5$
			$P' < 0.001$	$P' < 0.01$	$P' > 0.05$	$P' > 0.4$	$P' > 0.05$	$P' > 0.05$	$P' > 0.3$	$P' > 0.8$

$n = 8$ in each group, P—probability of difference compared to the norm, P'—compared to the group 2a and 2b

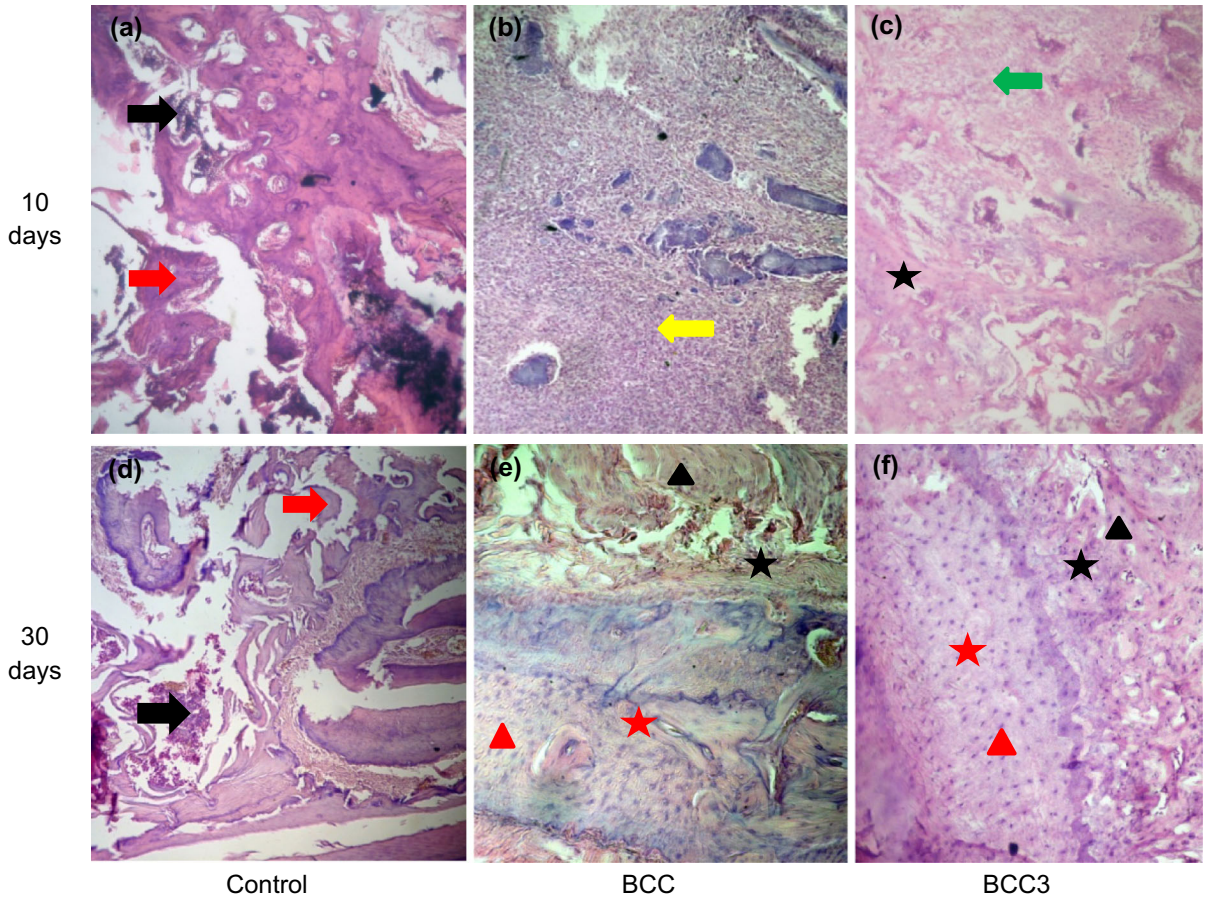

Fig. 8 H&E staining of bone defect empty (**a, d**), with BCC (**b, e**), and BCC3 (**c, f**) at 10 and 30 days post-implantation. Micrographs, ×40–×70. *Notes Red arrow* bone destruction, *black arrow* fibrous tissue with blood imbibition, *yellow arrow* multicellular granulation tissue and giant cells, *green arrow* bone tissue homogenization, *red triangle* osteoblasts, *black triangle* fibroblasts, *red star* newly formed sites of well-vascularized bone, *black star* connective tissue structures. *Abbreviations BCC* bioactive ceramic composite, *BCC3* bioactive ceramics composite doped 1 at.% Ag and 0.5 at.% Cu, *H&E* hematoxylin and eosin. (Color figure online)

Bone defect reparation

Alveolar bone tissue of normal structure without any peculiarities was found in histological specimen of intact rat group.

Biochemical and morphological data obtained from the bone tissue defect area show substantial rise in phosphatase activity on the 10th day primarily due to alkaline phosphatase, which tends to become normal only about 30 days after the experimental defect formation. Nevertheless, on the 30th day, AlP activity in rats of the 2nd group with unfilled bone defect decreases, whereas in the groups where BCC was used AlP activity remained high. When created, the bone defect causes considerable increase of GPA and tends to stimulate elastase activity, but only at the early stage as are represented in Table 4.

Content of dissolved bone protein was not appreciably changed after the defect formation though the tendency to growth was visible as early as within the first 10 days, whereas filling the defect with BCC causes to return the values to normal by the 30th day. The bone tissue calcium content in the defect area significantly decreases and does not visibly change in the presence of bone grafts; the same occurs also with the phosphorus content (Table 4).

In the second rat group, calcium and phosphorus contents go down, while calcium content to dissolved

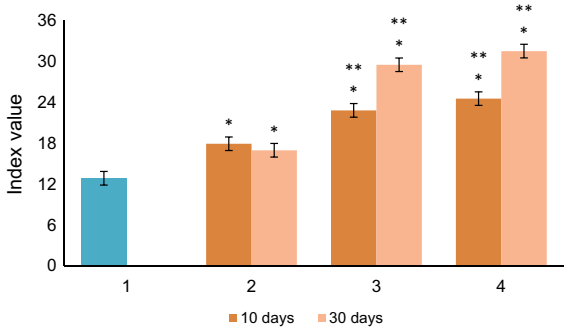

Fig. 9 Distribution of MI at the involved bone sites *Abbreviations* 1—norm, 2—bone defect (BD), 3—BD with BCC, 4—BD with BCC3 *Notes* *—$P < 0.05$ compared to the group 1, **—$P < 0.05$ compared to the group 2

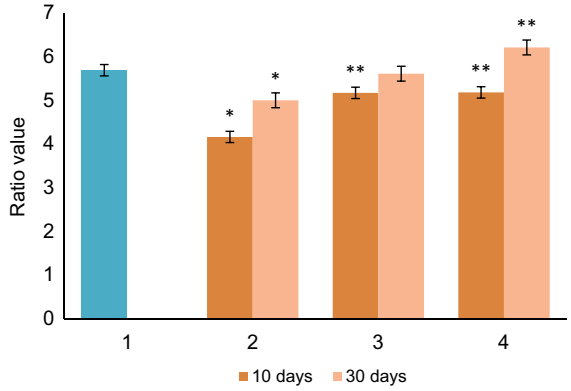

Fig. 10 Distribution of mineral/protein substances ratio in the alveolar bone *Abbreviations* 1—norm, 2—bone defect (BD), 3—BD with BCC, 4—BD with BCC3 *Notes* *—$P < 0.05$ compared to the group 1, **—$P < 0.05$ compared to the group 2

protein ratio noticeably decreases. In the same rat group, pathomorphological evidence of bone lamella destruction in histological specimens is observed on the 10th day. Some bone tissue fragments are subject to necrosis and they have been surrounded by dense patches of connective tissue with focal hemorrhages, osteocyte degeneration being observed. The destruction process gives rise to the formation of hollows in the bone tissue (Fig. 8a). Ongoing inflammatory reaction accompanied by tenuous signs of bone reparation can be evident on the 30th day (Fig. 8d).

Thus, no evidence of initial reparative process or bone tissue formation has been registered one month following the creation of experimental defect.

However, it should be noted that BCC grafts both Ag/Cu-doped and undoped improve bone tissue reparation properties. AlP activity significantly grows ($P < 0.05$) proving osteoblast stimulation. Furthermore, the mineralization index (MI) rises by the 10th day of experiment in both ceramic samples presence (Fig. 9). BCC samples considerably decrease GPA (in most cases to normal values); however, they scarcely affect the increased elastase level. Therefore, GPA/elastase ratio growing as the bone defect was created decreases considerably ($P < 0.05$) under the influence of bone grafts with no palpable differences between ceramics samples (Table 4). Nonetheless, the histological view displays inflammatory condition with lymphoid infiltration (Fig. 8b, c). Partial resorption of bone tissue decay products along with multicellular connective tissue resembling granulation tissue with gigantic cells can be observed. As bone tissue homogenizes, the number of osteoblasts significantly decreases or they are absent. By the 30th day of experiment, the biochemical values become normal with persistently high mineralization index. Significantly low Ca/prot. ratio, which creates after bone defect formed, returns to the normal value under the influence of ceramic samples on the 10th day (group 1) and on the 30th day under the influence of BCC3, and it even slightly exceeds the normal rate (Fig. 10). Histological analysis on the 30th day in the 3rd and 4th groups shows signs of reparative bone regeneration at the microscopic level (Fig. 8e, f). In this term, sites of quite well-grown bone tissue can be found near those of immature but well-vascularized osteoid tissue. The number of osteoblasts rises, and osteocytes are uniformly arranged and surrounded by plenty of intercellular substance. No inflammatory evidences can be observed in both experimental groups.

Thus, the investigation carried out demonstrates that bioactive ceramics can stimulate osteogenesis mainly affecting the mineralization function, which is proved by significant ($P < 0.05$) rise in MI at each experimental time and Ca/prot. ratio normalization by the 30th day. The characteristic of pathomorphological changes on the 10th day following the defect creation without or with use of bioactive ceramics is similar. Nonetheless, 1 month after bone grafting the morphological view was different from that in the control rat group. If the former is the case of ongoing bone lamella destruction alongside slightly expressed bone element regeneration or their replacement by dense fibrous tissue, then the latter showed more apparent substitutive reparation owing to bioactive ceramics. Moreover, the signs of inflammatory

reaction were virtually absent in this case. Bone lamella reparation or destruction area substitution by connective tissue and sufficiently vascularized de novo formed bone tissue could be observed (Gerard et al. 2010). It should be noted that applying silver- and copper-doped BCC or undoped one does not lead to any significant quantitative and qualitative difference in terms of biochemical and morphological aspects of experimental defect reparation.

Conclusion

For proposed variant of multiphase nanostructured BCC containing Zn, doping the BCC granules with Ag (0.1–10 at.%) and Cu (0.05–5 at.%) at 2:1 ratio imparts to the bioactive ceramics antibacterial, antifungal, and cytotoxic properties. These properties are directly dependent on the concentration of silver and copper embedded into the crystal lattice of the HAp-TCP nanostructured granules. The BCC containing 0.5–1 at.% silver and 0.25–0.5 at.% copper seems to be the most promising in terms of future application. Such BCC exhibits satisfactory antimicrobial properties and does not hinder human cell growth in vitro. In vivo grafting the BCC doped with 1 at.% silver and 0.5 at.% copper revealed no evidence of bone regeneration stunting. On the contrary, there was a tendency to intensify bone regenerate mineralization. This variant of the BCC could be considered as the synthetic bone substitute of choice in various clinical cases especially in those demanding anti-inflammatory impact. Nevertheless, further thorough research including comprehensive clinical studies is necessary.

Acknowledgments The authors gratefully acknowledge the support of Dr. Olena Voloshuk from Bogomolets National Medical University (Ukraine), the Department of Microbiology, Virology, and Immunology. Dmytro Zubov, leading researcher and Roman Vasyliev, researcher from State Institute of Genetic and Regenerative Medicine of NAMS (Ukraine), in the implementation phases of the study. We express profound gratitude to Prof. Anatolii Levitskyi for the access to biochemical laboratory and vivarium facilities at State Institute of Stomatology of NAMS (Odesa, Ukraine). This project is financially supported by Branch target preparation Kyiv National Taras Shevchenko University, NAMS of Ukraine (Grant No. 0114U003876).

Conflict of interest The authors have no financial interest in any of the companies or products, devices, and biomedical preparation mentioned in this manuscript. Therefore, authors have no conflict of interests.

References

Balagna C, Vitale-Brovarone C, Miola M, Verné E, Canuto RA, Saracino S, Muzio G, Fucale G, Maina G (2011) Biocompatibility and antibacterial effect of silver doped 3D-glass-ceramic scaffolds for bone grafting. J Biomater Appl 25(6):595–617. doi:10.1177/0885328209356603

Balamurugan A, Balossier G, Laurent-Maquin D, Pina S, Rebelo AH, Faure J, Ferreira JM (2008) An in vitro biological and anti-bacterial study on a sol-gel derived silver-incorporated bioglass system. Dent Mater 24(10):1343–1351. doi:10.1016/j.dental.2008.02.015

Bancroft JD, Stevens A (1990) Theory and practice of histological techniques, 2nd edn. Churchill Livingstone, London

Barralet J, Gbureck U, Habibovic P, Vorndran E, Gerard C, Doillon CJ (2009) Angiogenesis in calcium phosphate scaffolds by inorganic copper ion release. Tissue Eng Part A 15(7):1601–1609. doi:10.1089/ten.tea.2007.0370

Chen W, Oh S, Ong AP, Oh N, Liu Y, Courtney HS, Appleford M, Ong JL (2007) Antibacterial and osteogenic properties hydroxyapatite coatings produced using of silver-containing a sol gel process. J Biomed Mater Res Part A 82A:899–906

Chen J, Wang Y, Chen X et al (2011) A simple sol-gel technique for synthesis of nanostructured hydroxyapatite, tricalcium phosphate and biphasic powders. Mater Lett 65:1923–1926. doi:10.1016/j.matlet.2011.03.076

Daculsi G, Laboux O, Malard O, Weiss P (2003) Current state of the art of biphasic calcium phosphate bioceramics. J Mater Sci Mater Med 14:195–200

Dodwad V, Vaish S, Mahajan A, Chhokra M (2012) Local drug delivery in periodontics: a strategic intervention. Int J Pharm Pharm Sci 4(4):30–34

Dominici M, Le Blanc K, Mueller I, Slaper-Cortenbach I, Marini F, Krause D, Deans R, Keating A, Prockop DJ, Horwitz E (2006) Minimal criteria for defining multipotent mesenchymal stromal cells. The international society for cellular therapy position statement. Cytotherapy 8(4):315–317

Dorozhkin SV (2010) Nanosized and nanocrystalline calcium orthophosphates. Acta Biomater 6(3):715–734. doi:10.1016/j.actbio.2009.10.031

Eniwumide JO, Yuan H, Cartmell SH, Meijer GJ, de Bruijn JD (2007) Ectopic bone formation in bone marrow stem cell seeded calcium phosphate scaffolds as compared to autograft and (cell seeded) allograft. Eur Cells Mater 14:30–39

Ewald A, Käppel C, Vorndran E, Moseke C, Gelinsky M, Gbureck U (2012) The effect of Cu(II)-loaded brushite scaffolds on growth and activity of osteoblastic cells. J Biomed Mater Res A 100(9):2392–2400. doi:10.1002/jbm.a.34184

Fan J, Lei J, Yu C, Tu B, Zhao D (2007) Hard-templating synthesis of a novel rod-like nanoporous calcium

phosphate bioceramics and their capacity as antibiotic carriers. Mater Chem Phys 103(2–3):489–493
Gerard C, Bordeleau LJ, Barralet J, Doillon CJ (2010) The stimulation of angiogenesis and collagen deposition by copper. Biomaterials 31(5):824–831
Gupta A, Phung LT, Taylor DE, Silver S (2001) Diversity of silver resistance genes in IncH incompatibility group plasmids. Microbiology 147:3393–3402
Hammond JS, Gaarenstroom SW, Winograd N (1975) X-ray photoelectron spectroscopic studies of cadmium- and silver-oxygen surfaces. Anal Chem 47:2193–2199. doi:10.1021/ac60363a019
Heitz-Mayfield L, Tonetti MS, Cortellini P, Lang NP, European Research Group on Periodontology (ERGOPERIO) (2006) Microbial colonization patterns predict the outcomes of surgical treatment of intrabony defects. J Clin Periodontol 33(1):62–68
Hsu YH, Turner IG, Miles AW (2007) Fabrication of porous bioceramics with porosity gradients similar to the bimodal structure of cortical and cancellous bone. J Mater Sci Mater Med 18:2251–2256
International Organization for Standardization (ISO) (2009) Biological evaluation of medical devices, ISO 10993—part 5: tests for in vitro cytotoxicity. International Organization for Standardization, Geneve
Jaiswal S, McHale P, Duffy B (2012) Preparation and rapid analysis of antibacterial silver, copper and zinc doped sol-gel surfaces. Colloids Surf B 94:170–176
Landi E, Logroscino G, Proietti L, Tampieri A, Sandri M, Sprio S (2008) Biomimetic Mg-substituted hydroxyapatite: from synthesis to in vivo behaviour. J Mater Sci Mater Med 19:239–247
Lüthen F, Bergemann C, Bulnheim U et al (2010) A dual role of copper on the surfaces of bone implants. Mater Sci Forum 638–642:600–605
Marambio-Jones C, Hoek EMV (2010) A review of the antibacterial effects of silver nanomaterials and potential implications for human health and the environment. J Nanopart Res 12:1531–1551. doi:10.1007/s11051-010-9900-y
Munch E, Franco J, Deville S, Hunger P, Saiz E, Tomsia AP (2008) Porous ceramic scaffolds with complex architectures. JOM 60(6):54–58
O'Donnell MD, Fredholm Y, de Rouffignac A, Hill RG (2008) Structural analysis of a series of strontium-substituted apatites. Acta Biomater 4:1455–1464
Parmigiani F, Pacchioni G, Illas F, Bagus PS (1992) Studies of the CuO bond in cupric oxide by X-ray photoelectron spectroscopy and ab initio electronic structure models. J Electron Spectrosc Relat Phenom 59:255–269. doi:10.1016/0368-2048(92)87005-7
Porter AE, Botelho CM, Lopes MA, Santos JD, Best SM, Bonfield W (2004) Ultrastructural comparison of dissolution and apatite precipitation on hydroxyapatite and silicon-substituted hydroxyapatite in vitro and in vivo. J Biomed Mater Res 69A(4):670–679
Rameshbabu N, Sampath Kumar TS, Prabhakar TG, Sastry VS, Murty KV, Prasad Rao K (2007) Antibacterial nanosized silver substituted hydroxyapatite: synthesis and characterization. J Biomed Mater Res A. 80(3):581–591
Rodriguez JP, Rios S, Gonzalez M (2002) Modulation of the proliferation and differentiation of human mesenchymal stem cells by copper. J Cell Biochem 85(1):92–100
Sanchez-Salcedo S, Izquierdo-Barba I, Arcos D, Vallet-Regio M (2006) In vitro evaluation of potential calcium phosphate scaffolds for tissue engineering. Tissue Eng 12:279–290
Schön G, Tummavuori J, Lindström B et al (1973) ESCA Studies of Ag, Ag_2O and AgO. Acta Chem Scand 27:2623–2633. doi:10.3891/acta.chem.scand.27-2623
Shanmugam S, Gopal B (2014) Copper substituted hydroxyapatite and fluorapatite: synthesis, characterization and antimicrobial properties. Ceram Int 40(10):15655–15662. doi:10.1016/j.ceramint.2014.07.086
Shepherd JH, Shepherd DV, Best SM (2012) Substituted hydroxyapatites for bone repair. J Mater Sci Mater Med 23(10):2335–2347. doi:10.1007/s10856-012-4598-2
Sogo Y, Ito A, Fukasawa K, Sakurai T, Ichinose N (2004) Zinc containing hydroxyapatite ceramics to promote osteoblastic cell activity. Mater Sci Technol 20(9):1079–1084. doi:10.1179/026708304225019704
Spence G, Patel N, Brooks R, Rushton N (2009) Carbonate substituted hydroxyapatite: resorption by osteoclasts modifies the osteoblastic response. J Biomed Mater Res 90A(1):217–224
Stoscheck CM (1990) Quantitation of protein. Methods Enzymol 182:50–69
Thanyaphoo S, Kaewsrichan J (2012) Synthesis and evaluation of novel glass ceramics as drug delivery systems in osteomyelitis. J Pharm Sci 101(8):2870–2882. doi:10.1002/jps.23230
Wu C, Zhou Y, Xu M, Han P, Chen L, Chang J, Xiao Y (2013) Copper-containing mesoporous bioactive glass scaffolds with multifunctional properties of angiogenesis capacity, osteostimulation and antibacterial activity. Biomaterials 34(2):422–433. doi:10.1016/j.biomaterials.2012.09.066
Xing ZC, Chae WP, Baek JY, Choi MJ, Jung Y, Kang IK (2010) In vitro assessment of antibacterial activity and cytocompatibility of silver-containing PHBV nanofibrous scaffolds for tissue engineering. Biomacromolecules 11(5):1248–1253. doi:10.1021/bm1000372